The Semi-direct Aerosol Effect: Impact of Absorbing Aerosols on Marine Stratocumulus

By B. T. JOHNSON,[1*] K. P. SHINE, and P. M. FORSTER
Department of Meteorology, University of Reading, UK

(Revised October 2003, awaiting acceptance, please do not cite or copy without permission)

SUMMARY

Aerosols that absorb solar radiation may lead to a decrease of low cloud cover and liquid-water path (LWP) leading to a positive radiative forcing. A Large-Eddy Model is used to investigate this 'semi-direct effect' for marine stratocumulus and examine the dependency on the vertical distribution of the aerosol. In this study the aerosols influence clouds by directly altering the shortwave heating rate (the semi-direct effect), but do not interact with cloud microphysics (i.e. indirect aerosol effects are excluded). Absorbing aerosols within the boundary layer (BL) decreased LWP by 10 g m^{-2} leading to a positive semi-direct forcing. Even for mildly absorbing aerosols (mid-visible single scattering albedo of 0.96) the semi-direct forcing was three times stronger, and opposite in sign to the aerosol direct forcing. The semi-direct forcing is found to be proportional to aerosol single scattering co-albedo (tested to a value of 0.12). Conversely, with the absorbing aerosol layer above the cloud, the LWP increased by 5-10 g m^{-2} leading to a negative semi-direct forcing. Absorbing aerosols located in the BL heat the cloud layer enhancing the daytime decoupling and thinning of stratocumulus layer. Absorbing aerosols immediately above the BL increase the contrast in potential temperature across the inversion leading to a lower cloud-top entrainment rate. With aerosol both within and above the BL the semi-direct forcing was positive but half the magnitude of when aerosol was only in the BL. As marine stratocumulus cover about 20% of the globe, the semi-direct effect could significantly influence the radiative forcing by absorbing aerosols.

KEYWORDS: Boundary layer Large-Eddy-Simulation Radiative forcing

1. INTRODUCTION

Aerosols have a significant impact on the earth's radiation budget by scattering and absorbing solar radiation. Aerosols are mainly comprised of non-absorbing material such as sulphates, nitrates and organic carbon (e.g. Pilinis *et al.* 1995) which scatters solar radiation back to space leading to a negative radiative forcing, i.e. a cooling of the climate system. Aerosols can also contain absorbing material, principally black carbon (soot) from the burning of biomass and fossil fuels, and also dust from arid regions. This leads to a positive radiative forcing that partly offsets aerosol scattering effects (IPCC 2001).

In addition, aerosol absorption may decrease low cloud cover by heating the air and reducing relative humidity. This leads to a positive radiative forcing, termed the 'semi-direct effect', which amplifies the warming influence of absorbing aerosols (Hansen *et al.* 1997). This process is distinct from both the direct aerosol effect (scattering and absorption), and the indirect aerosol effect whereby aerosols increase cloud albedo and lifetime via microphysical interactions leading to a negative radiative forcing (Haywood and Boucher 2000). Aerosol absorption also decreases the absorbed solar radiation at the surface and increases low-level static stability leading to lower surface moisture fluxes (Ramanathan *et al.* 2001). This could also reduce cloud cover, or the probability of cloud formation. Thus, absorbing aerosols could have a significant impact on regional and global climate, but the few global studies that have addressed or implicated the semi-direct aerosol effect lead to different conclusion on its relative importance.

In the simplified general-circulation model (GCM) study by Hansen *et al.* (1997), the climate sensitivity to absorbing aerosols (with mid-visible single scattering albedo of 0.80) was almost three times greater than the climate sensitivity to other forcings,

* Corresponding author: Department of Meteorology, University of Reading, Earley Gate, PO Box 243, Reading, Berkshire, RG6 6BB, UK. **Email: b.t.johnson@rdg.ac.uk**

such as a doubling of the concentration of CO_2. Similar results were found by Cook and Highwood (2003), using an Intermediate GCM, and by Jacobson (2002), using a more sophisticated GCM with detailed emissions and treatment of aerosol processes. In Jacobson's model the climate was more than twice as sensitive to the (positive) direct radiative forcing from fossil-fuel related, black carbon and organic matter aerosols, than to the radiative forcing from increased concentrations of greenhouse gases CO_2 and CH_4. These studies imply that reductions in low cloud cover contribute significantly to the warming influence of absorbing aerosols. In contrast, using the ECHAM4 general-circulation model with a coupled aerosol-chemistry module, Lohmann and Feichter (2001) found that the global annual mean semi-direct forcing was negligible (0.1 W m^{-2}), even for columns with a relatively high black carbon burden (> 2 mg m^{-2}). Although there were significant reductions of liquid-water path (LWP) in highly polluted regions (up to 10 g m^{-2}), the global average LWP increased due to the indirect aerosol effect. It was noted, however, that there was an uncertainty factor of 2 in the emission data for black carbon. Also, the radiative properties of aerosols were based on external mixtures, whereas internal mixtures may absorb 2 - 2.5 times more shortwave radiation (e.g. Chylek *et al.* 1996). A recent study (Penner *et al.* 2003) using a coupled chemical transport model and GCM reports a negative semi-direct forcing from fossil-fuel-related carbonaceous aerosol and biomass burning aerosols. However, their "forcing" included a component of longwave response due to changes in land surface temperature, and consequent changes in tropospheric temperature. It is not clear that these adjustments should be counted as the semi-direct effect. Considering only changes in cloud cover, the semi-direct forcing would have been positive due to reductions of stratiform and convective clouds.

These studies (Hansen *et al.* (1997); Lohmann and Feichter (2001); Jacobson (2002); Cook and Highwood (2003); Penner *et al.* (2003)) illustrate that models generate a semi-direct effect, but as yet it is not clear how important the semi-direct effect is compared to other aerosol effects, for example, the indirect effect, and other climate forcings. Also, these studies revealed little about the mechanisms associated with the semi-direct effect that are responsible for the changes in cloud amounts and LWP. The complexity of cloud dynamics itself suggests that the mechanisms of the semi-direct effect are likely to depend, to a large extent, on local meteorological conditions.

Large-Eddy-Simulations which explicitly resolve clouds and large turbulent eddies offer the opportunity to increase our understanding of the semi-direct aerosol effect by examining the response on local scales. For example, Ackerman *et al.* (2000) used this method to show that the dark regional haze observed during the Indian Ocean Experiment (INDOEX) hastened the daytime clearing of cumulus cloud over the Indian Ocean. The absorbing aerosol reduced the relative humidity leading to more rapid detrainment of the cumulus clouds, especially where they spread out beneath the inversion. The solar heating was maximum at cloud-top and increased the stability of the boundary layer (BL), reducing daytime cloud fraction by 5-10%. However, other cloud regimes have not yet been considered.

Marine stratocumulus have a major role in the climate system because of their high global coverage over subtropical oceans and their high albedo compared to the ocean. These clouds commonly form near the western coastline of continents and at times may be subject to high concentrations of continental aerosols. For example, polluted air from Europe was observed over the north-east Atlantic during the Atlantic Stratocumulus Transition Experiment (ASTEX) (Huebert *et al.* 1996) and the second Aerosol Characterisation Experiment (ACE-2) (Johnson *et al.* 2000a). The Southern African Regional Science Initiative (SAFARI-2000) also revealed deep layers of highly absorbing biomass

burning aerosol over the south-eastern Atlantic stratocumulus regions (Haywood *et al.* 2003). In this paper we use the UK Met Office Large-Eddy Model (LEM) to simulate a marine stratocumulus-capped BL and explore the semi-direct aerosol effect using idealised aerosol distributions. Two particular dependencies are studied: one is the dependence on the aerosol single scattering albedo (section 3), the other is the vertical location of the aerosol relative to the inversion (section 4).

2. THE LARGE-EDDY MODEL

The LEM is a 3D high-resolution numerical model with periodic lateral boundary conditions (Mason 1989; Gray *et al.* 2001). The resolved flow, which includes large turbulent eddies is solved using a filter operation to the Navier Stokes equations (Brown 1999). Small-scale turbulence is represented by first-order turbulence closure in the subgrid model. The model uses the conserved scalars total water mixing ratio (Q_t) and the liquid water potential temperature (θ_l) where $Q_t = Q_v + Q_l$ and $\theta_l = \theta - (LQ_l/C_p)$. Q_v is the water vapour mixing ratio, Q_l is the liquid water mixing ratio, L is the latent heat of evaporation, C_p is the specific heat capacity and θ is the potential temperature. The liquid water mixing ratio, Q_l is diagnosed at each grid point as $Q_l = Q_t - Q_{sat}$, for $Q_t > Q_{sat}$ where Q_{sat} is the local saturation mixing ratio. In these simulations precipitation processes were neglected because the liquid water content was too low for these to have any significant influence.

Surface fluxes are calculated using Monin-Obukhov similarity with a no-slip surface and using a specified sea surface temperature. The top boundary is a stress-free rigid lid. The temperature in the top 200 m of the model is relaxed to the initial conditions with a 3-hour time-scale to prevent drift of the temperature with time. The relaxation also prevents reflection of gravity waves.

The LEM is used to simulate a typical example of subtropical marine stratocumulus based on observations from the First International Satellite Cloud Climatology Project Regional Experiment (FIRE) (Hignett 1991), which took place off the coast of California in July 1987. Some aspects of the model set-up are guided by the intercomparison study by the EUROpean project on Cloud Systems in climate models (EUROCS): stratocumulus over the ocean (Duynkerke *et al.* 2000), and European Centre for Medium-Range Weather Forecasts (ECMWF) reanalysis data. The initial conditions (Table 1) are based on 6 radiosonde ascents taken through a stratocumulus layer during FIRE (Duynkerke and Hignett 1993). Total water and liquid water potential temperature are constant in the BL, representing a well-mixed layer, and there is a very strong potential temperature inversion of 12 K at 600 m. Cloud top coincides with the inversion height and the cloud base was initially at 250 m giving a 350 m thick cloud layer with a LWP of 110 g m^{-2}. Sea surface temperature is fixed at 288 K and the surface roughness length was 2 x 10^{-4} m. The surface pressure is fixed at 1012.5 mb and the large-scale pressure gradient is specified to give a zonal geostrophic wind, U_g of 6.0 m s^{-1} and a meridional geostrophic wind, V_g of -1.0 ms^{-1} (based on ECMWF reanalysis data for July 1987). The winds were set to geostrophic values at the initial time. The subsidence rate, (W_{subs}) was given by $W_{subs} = \int Ddz$, where z is height and D, the large-scale divergence rate was specified as 5.5 x 10^{-6} s^{-1} (Duynkerke *et al.* 2000). The subsidence rate at the inversion roughly balances the entrainment rate so that the inversion height does not drift significantly with time. A cooling of 1 K day^{-1} is applied to account for large-scale heat divergence as calculated from monthly mean reanalysis data for July 1987 from the National Centers for Environmental Prediction (NCEP). Large-scale moisture divergence was not included since this would have led to unrealistically low LWP.

TABLE 1. INITIAL CONDITIONS AND AEROSOL MASS MIXING RATIO

Height(m)	θ_l(K)	Q_t(g kg^{-1})	Aerosol mass mixing ratio (kg kg^{-1})
0	287.5	9.6	3x10^{-8}
595	287.5	9.6	3x10^{-8}
605	299.5	6.6	3x10^{-8}
900	301.75	6.6	0.0
1600	304.0	6.6	0.0

The horizontal resolution was 50 m and the domain size was 2.5 km x 2.5 km in experiment 1 and was reduced to 1.6 km x 1.6 km in experiment 2 to reduce the computational expense. There were 80 levels in the vertical between 0 and 1200 m and the resolution was variable, ranging from 20 m in the sub-cloud layer to 7 m near the inversion and up to 50 m near the model top. The enhancement of resolution at the inversion helped to better resolve the structure of the inversion, the cloud-top generation of turbulence, and the entrainment process. The time step was variable but averaged 0.15 seconds. In experiment 2, eight extra levels were inserted increasing the model top from 1200 to 1600 m to allow for a deep aerosol layer.

The two-stream radiation scheme coupled to the LEM has 6-bands in the shortwave and 8-bands in the longwave (Edwards and Slingo 1996). It was set to latitude 33^{o}N and 15 July, consistent with the location and date of the FIRE observations. Thus the radiative forcings in this paper relate to the summer season rather than annual averages. Aerosols were represented by a dry external mixture of soot and ammonium sulphate. Wavelength-dependent optical properties for dry ammonium sulphate and soot are from WCP (1986). The mass ratio of soot to ammonium sulphate was varied to give aerosol mixtures with a range of mid-visible single scattering albedos (ω): 0.88, 0.92, 0.96, and 1.00 (pure ammonium sulphate) †. This approximately covers the typical range of observed mid-visible ω values (e.g. Heintzenberg *et al.* (1997)). The aerosols are not advected within the model but idealised vertical distributions of aerosol mass mixing ratio are specified to represent BL aerosols, an aerosol layer above the BL, and a deep aerosol layer from the surface to 1.6 km. The range of vertical distributions are not specifically based on observations but are designed to investigate the influence of placing aerosols at different levels relative to the BL. In these simulations indirect effects are neglected; aerosols do not interact with the cloud microphysical or single scattering radiative properties.

3. EXPERIMENT 1: SENSITIVITY TO SINGLE SCATTERING ALBEDO

(*a*) *Experimental set-up*

To obtain a first estimate for the semi-direct aerosol effect we assume that the aerosol mass mixing ratio is constant in the BL (0-600 m) and reduces linearly to zero 300m above the inversion (Table 1). In experiment 1, there are four aerosol simulations, and an aerosol-free control simulation (Table 2). In each aerosol simulation the aerosol mass mixing ratio is kept constant but the ratio of soot to ammonium sulphate varies giving a range of single scattering albedos. Experiment 1-088 is the most absorbing aerosol simulation with ω = 0.88, experiments 1-092 and 1-096 have intermediate value of ω = 0.92 and 0.96, respectively, and experiment 1-100 has purely scattering aerosols (ω = 1.00). These reflect the typical range of mid-visible ω values observed

† Throughout this paper values of ω and optical depth (τ) given are for a mid-visible wavelength of 0.55μm. Single scattering albedos are optical depth weighted averages.

in marine environments (e.g. Satheesh and Ramanathan (2000); Russell (2002)). The aerosol optical depth (τ) is approximately 0.15 to represent highly polluted conditions. The simulations are started at 0600 h (just after dawn) on 15 July and run for 42 hours, ending at midnight on the second day. The first day of simulation is intended as spin-up period during which the BL structure evolves and LWP declines. The semi-direct forcings for day 2 are considered to be more representative but we show results for day 1 (Table 2) as an indication of inter-day variability.

(*b*) *Results of experiment 1*

The characteristics of the marine stratocumulus simulated by the LEM compare well with observations taken from San Nicolas Island (33.3°N, 119.5°W) during FIRE, July 1987 (Hignett 1991; Betts 1990). For instance, the mean value and diurnal range of cloud top height, cloud base height and LWP are consistent with the celiometer and sodar measurements (Duynkerke and Hignett 1993), and microwave radiometer estimates (Duynkerke and Teixeira 2001). Cloud thickness and LWP decline due to solar heating (Fig. 1(a)) from around 350 m and 90 g m^{-2} at dawn to 200 m and 30 g m^{-2} in the afternoon, respectively (Fig. 2). The addition of absorbing aerosols in the LEM experiment leads to a more rapid daytime thinning of the cloud (Fig. 2) due to the additional shortwave heating, which exceeds 3 K day^{-1} at 1200 h (Fig. 1(b)) compared to the shortwave heating in the control simulation, which reaches 20 K day^{-1} falling to 2 K day^{-1} in the sub-cloud layer (Fig. 1(a)) at 1200 h. Cloud fraction remains 100% because there is insufficient horizontal inhomogeneity to break up the layer.

(i) *Impact of solar radiation on cloud, turbulence and BL structure*

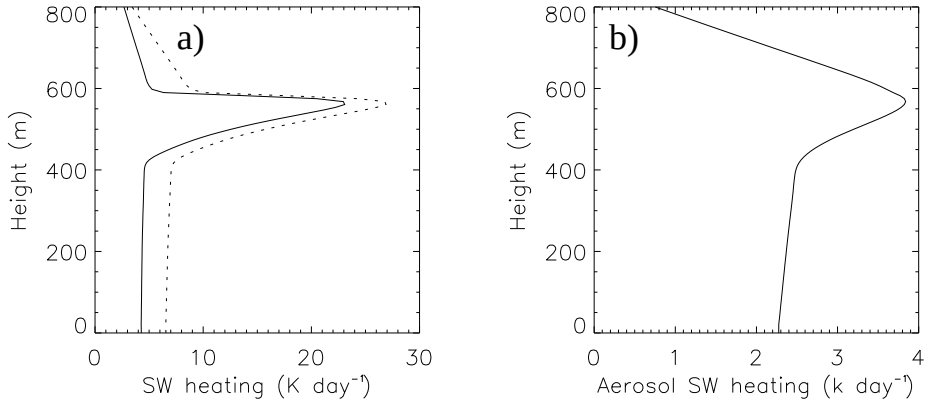

Figure 1. a) Shortwave heating rate (K day^{-1}) in experiment 1-088 (ω = 0.88) at 1200 h on day 2 with aerosols (dotted line), and without (solid line) aerosols included in the radiation calculation. b) Aerosol heating rate (K day^{-1}) in experiment 1-088, at 1200 h on day 2. This is the difference between heating rates calculated with and without aerosols.

During the daytime the BL stabilizes (Fig. 3(a)) because the solar heating is greater in the cloud layer, peaking at cloud-top (Fig. 1(a)). This leads to decoupling (e.g. Nicholls 1984), whereby turbulent fluxes, for example fluxes of moisture (Fig. 3(d)), between the surface and the cloud layer are greatly reduced. This leads to the drying of the cloud layer during the daytime (Fig. 3(b)), which explains the drop in LWP (Fig. 2(a)). The high solar heating rate at cloud-top also offsets the generation of turbulence

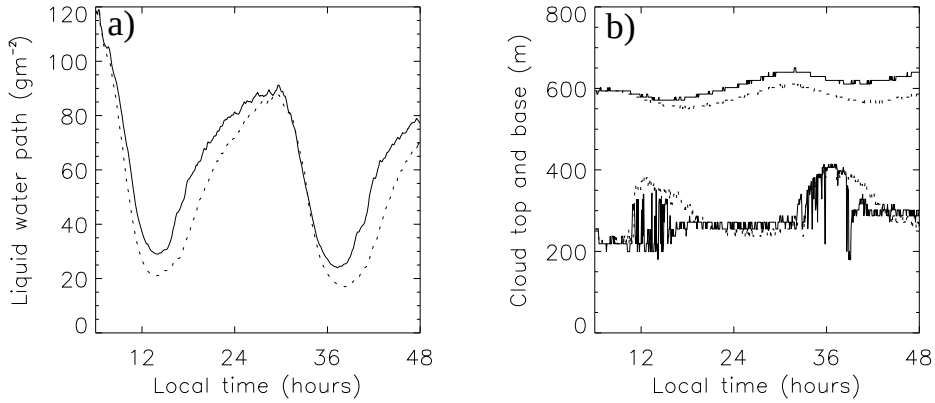

Figure 2. a) Liquid water path (gm^{-2}) and b) cloud top and cloud base (m), for the control simulation (solid line), and experiment 1-088, which has ω = 0.88 (dotted line).

by cloud-top longwave cooling. This contributes to the reduction of turbulence (Fig. 3(c)) and a lower entrainment rate, as indicated from the decline of the inversion height (Fig. 2(b)) and the decline in moisture flux at the cloud top (Fig. 3(d)). Moisture levels in the cloud layer decline despite this reduction of the entrainment rate because of the large reduction of moisture transport into the cloud from below, as indicated by the local minimum in turbulent moisture fluxes, which roughly coincides with the cloud base (Fig. 3(d)).

Although the heating from the absorbing aerosols has a significantly different vertical distribution to the solar heating in the aerosol-free BL (Fig. 1) it leads to similar changes in the BL structure. It warms and enhances the stability of the cloud layer, leading to a greater daytime reduction of moisture fluxes than in the control simulation (Fig. 3(d)). The cloud top height is also significantly lower in the absorbing aerosol simulation (Fig. 2(b)) indicating a lower entrainment rate. This is probably due to the lower LWP (Fig. 2(a)). The LWP in stratocumulus layers largely determines the cloud-top longwave cooling rate, which is one of the main processes determining the entrainment rate (Lock and Macvean 1999; Moeng 2000). Sharp longwave cooling near the cloud top, just beneath the inversion generates negatively buoyant air parcels that sink through the cloud. This convection promotes turbulent mixing in the vicinity of the inversion leading to the entrainment of free tropospheric air into the boundary layer. Entrainment tends to dry the boundary layer, reducing LWP. Lower LWP then leads to a lower entrainment rate. In this way negative feedback between LWP and entrainment acts to restore the LWP, possibly preventing the complete disappearance of the cloud layer in the simulations.

(ii) *Semi-direct radiative forcing*

The semi-direct radiative forcing (Fig. 4) is the difference in net irradiance at the Top of the Atmosphere (TOA) between the simulation with aerosols, and the aerosol-free control simulation, due only to changes in cloud fields. To calculate the semi-direct forcing, the direct influence of the aerosols on TOA net irradiance (the direct forcing) is subtracted from the total change in TOA net irradiance (total forcing) between aerosol and control simulations: Semi-direct forcing = total forcing - direct forcing. The direct forcing was calculated in the aerosol simulation, i.e. using the cloud fields that had been

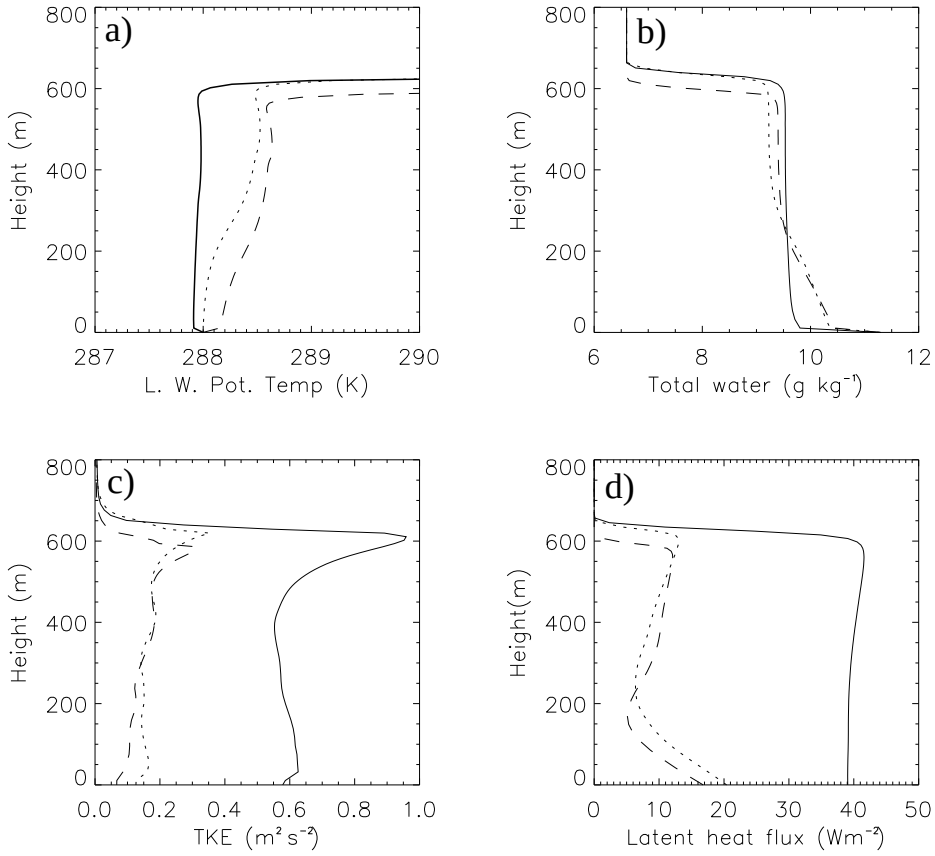

Figure 3. a) Liquid water potential temperature (K), b) total water (g kg^{-1}), c) turbulent kinetic energy (m^2 s^{-2}), and d) latent heat flux (W m^{-2}) on day 2 at 0500 (solid line) and 1200 h (dotted line) in the control simulation, and on day 2 at 1200 h (dashed line) in experiment 1-088.

modified by the aerosol heating. The semi-direct forcing is dominated almost entirely by the shortwave component; differences in outgoing longwave radiation are small because the cloud-top temperature is close to the sea surface temperature (5-6 K difference) and the cloud is optically quite thick at thermal infra-red wavelengths, even with a LWP down to 20 g m^{-2}. A maximum semi-direct forcing of 70 W m^{-2} occurs in experiment 1-088 around 1200 h on day 1 and 3900 h on day 2 (Fig. 4) when the solar insolation is near the diurnal maximum, and differences in LWP are greatest (Fig. 2).

Table 2 shows the diurnal average semi-direct, direct and total forcings for all four experiments. The semi-direct forcing is clearly dominant over the negative direct radiative forcing in this experiment. For example, the variation of the mean radiative forcing with ω, on day 2 is about 6 times greater for the semi-direct forcing than for the direct forcing (0.9 to 14.0 W m^{-2}), compared with -2.9 to -0.6 W m^{-2} (Table 2). This shows that direct absorption by the aerosols only contributes a small amount to the total change in absorbed solar radiation; the impact on cloud LWP is far more important.

Even for moderately absorbing aerosols (e.g. experiment 1-096, ω = 0.96) the semi-direct forcing is three times the magnitude of the direct forcing and has the opposite sign.

One contributor to the strength of the semi-direct effect in these experiments is that the cloud layers are close to the optically thin limit during the middle of the day. For example, τ = 4.5 and cloud albedo (α) = 0.25 in the control simulation, τ = 3 and, α = 0.18 in exp. 1-088 at 1400h. In the optically thin limit, the cloud albedo is most sensitive to differences in τ, or LWP. This maximises the semi-direct radiative forcing for a given difference in LWP. Had both cloud layers been much thicker the same difference in LWP would have resulted in a smaller semi-direct radiative forcing.

The semi-direct forcing has a different pattern on the second day (Fig. 4); it is small and negative for a few hours after dawn but rises sharply peaking about 3 hours later than on day 1. There are two reasons for these differences. Firstly, turbulence impacts on the temporal variation of LWP and therefore the semi-direct forcing. Secondly the evolution of the BL and cloud structure are slightly different in the absorbing aerosol simulation. The BL is shallower and moister than in the control because of the lower entrainment rate on the previous day. This leads to a higher nighttime LWP, which explains the period of negative semi-direct forcing after dawn on day 2. This also explains why the diurnal mean semi-direct radiative forcings are approximately 25% lower on day 2 than on day 1 (Table 2). In a ten-day long experiment (not shown) we found that the diurnal mean semi-direct forcing converges to about 60% of the day 1 value by the third or fourth day of simulation. However, in this paper the simulations are limited to 2 days, which is perhaps a more realistic time frame for studying the semi-direct response, since marine stratocumulus boundary layers are transient systems, and typical follow a transition to cumulus on time scales of a few days as they are advected over warmer sea surfaces (e.g. Krueger *et al.* 1995).

Figure 5 shows that the semi-direct effect increases linearly with decreasing ω in the range 1.00 to 0.88. However, a lower single scattering albedo, or a higher aerosol optical depth could lead to the complete evaporation of the cloud layer at which point the linearity of the relationship would break down. Using a linear interpolation (Fig. 5), the direct and semi-direct forcings would balance for $\omega = \omega_{**}$ = 0.985 (where ω_{**} is the critical single scattering albedo for the sum of the semi-direct and direct effects to be zero). Hence the total aerosol radiative forcing (excluding indirect effects) would be positive for $\omega < \omega_{**}$ = 0.985. In contrast we find that the direct radiative forcing is positive only for $\omega < \omega_* = 0.85$ (where ω_* is the critical single scattering albedo for the direct effect only). This is particularly important as values of $\omega < 0.85$ are only observed in highly polluted regions, for example during the Indian Ocean Experiment (Ramanathan *et al.* 2001) whereas it is common to observe values of $\omega < 0.985$ (IPCC 2001).

We find that the results do not vary considerably with horizontal domain size (from 1 km^2 to 6.25 km^2) or changes to the large-scale forcing (e.g. doubling the large-scale cooling rate). Groups of similar simulations (not shown) performed on a smaller domain (1 km x 1 km) suggest that inter-day variability and initial condition uncertainty contribute to an uncertainty of about +/- 2 W m^{-2} in diurnal mean semi-direct forcing. Thus, it seems these results are robust to changes in the experimental set-up.

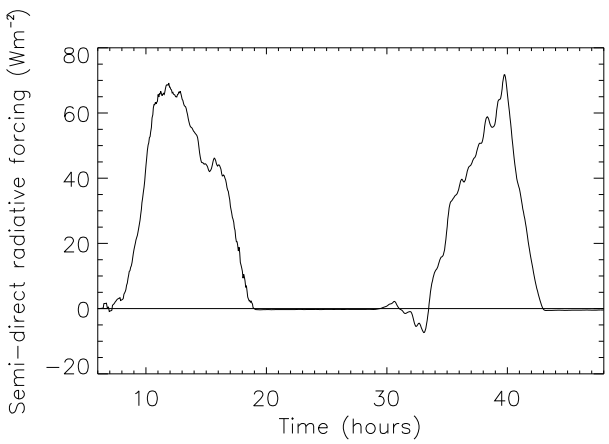

Figure 4. The semi-direct radiative forcing (W m^{-2}) as a function of time for experiment 1-088 (ω = 0.88).

TABLE 2. SUMMARY OF EXPERIMENT 1

Exp.	ω	Semi-direct		Direct	Total
		Day 1	Day 2	Day 2	Day 2
1-088	0.88	18.5	14.0	-0.6	13.4
1-092	0.92	13.0	10.4	-1.2	9.2
1-096	0.96	7.0	5.3	-2.0	3.3
1-100	1.00	-0.1	0.9	-2.9	-2.0

The diurnal mean semi-direct, direct and total aerosol radiative forcings (W m^{-2}) for different mid-visible aerosol single scattering albedos (ω) for day 2, and also the diurnal mean semi-direct forcing for day 1.

4. EXPERIMENT 2: SENSITIVITY TO VERTICAL DISTRIBUTION OF AEROSOLS

(*a*) *Experimental set-up*

Observations (Clarke *et al.* 1996; Johnson *et al.* 2000b) suggest that aerosol layers advected over the ocean are often much deeper than the marine BL, and may be located well above the BL (Haywood *et al.* 2003). Thus, a significant proportion of the aerosol mass can be above the local inversion. It is therefore important to consider whether aerosol above the stratocumulus-capped BL has any effect on the cloud LWP. In addition it is important to know whether there is linearity of response, i.e. if the sum of responses to aerosols above and below the inversion separately is the same as the response to an aerosol layer throughout both regions.

Four further simulations of the marine stratocumulus-capped BL are performed (Table 3). In each simulation the mass mixing ratio within the aerosol layer is fixed at 3 x 10^{-8} kg kg^{-1} , so that the aerosol heating rate within aerosol layers is similar in each experiment ($\sim$ 1 K day^{-1}). However, the vertical distributions vary (Table 3) and the aerosol optical depths also vary in proportion to the depth of the aerosol layers (Table 3). Absorbing aerosols have a ω of 0.88 at 0.55μm, as in experiment 1-088. A new aerosol-free control run was also performed because of differences in start time, domain size and the number of vertical levels between experiments 1 and 2.

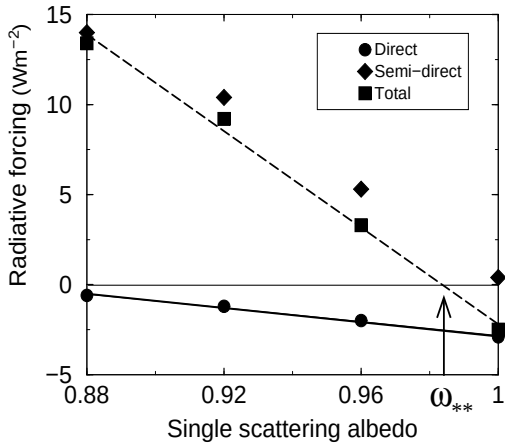

Figure 5. The diurnal mean direct, semi-direct and total aerosol radiative forcings (W m^{-2}) for day 2, with linear fits to the direct forcing (solid line) and total forcing (dashed line) as a function of mid-visible single scattering albedo. Numerical values also given in Table 2. ω_{**} is the critical single scattering albedo for which the total forcing is zero.

TABLE 3. SUMMARY OF EXPERIMENT 2

Experiment	Height range of aerosol layer	optical depth	Semi-direct	Direct	Total
2-BL Absorbing aerosol in BL	0 to Z_{inv}	0.12	22.8	-2.3	20.5
2-FT Absorbing aerosol above BL	Z_{inv} to 1.6 km	0.2	-9.5	10.2	0.7
2-BLFT Absorbing aerosol in and above BL	0 to 1.6 km	0.32	10.2	5.2	15.4
2-FTS Scattering aerosol above BL	Z_{inv} to 1.6 km	0.2	-0.1	-7.3	-7.4

The 2-day mean semi-direct, direct and total aerosol radiative forcings (W m^{-2}) for different aerosol layers. Z_{inv} is the height of the inversion, which varies between 600 and 650 m. Absorbing aerosol has ω = 0.88 (at 0.55μm) and scattering aerosol has ω = 1.00. The aerosol mass mixing ratio is 3x10^{-8}kg kg^{-1} in the aerosol layer.

The simulations were started at midnight, and the 5-6 hours before dawn are considered a spin-up period. This is different from the first experiment where simulations were started at 0600 h. The model top was extended from 1200 m to 1600 m with the addition of 8 extra levels to accommodate the deeper aerosol layers. Also, the height at which relaxation to initial conditions occurred was moved up from 1000 m to 1400 m. This was important to enable the air above the inversion to warm in response to heating from the aerosols. These changes had little effect on the LWP, or the structure and turbulent characteristics of the boundary layer. The simulations were run for 48 hours.

(*b*) *Results of experiment 2*

As shown in experiment 1, absorbing aerosols in the BL lead to a large positive semi-direct forcing (the mean of days 1 and 2 was 16 W m^{-2} in experiment 1-088 (Table 2)). In experiment 2-BL the 2-day mean semi-direct forcing was significantly higher (23 W m^{-2},Table 3), yet both experiments had the same ω and aerosol mass concentration. The lower value in experiment 1 was likely to be because there was some aerosol above the inversion, whereas in experiment 2-BL there was none above the inversion, as explained below.

Absorbing aerosols above the inversion (experiment 2-FT) enhance the LWP leading to negative semi-direct forcing of -9.5 W m^{-2} (Table 3). In experiment 2-FT the potential temperature above the inversion is 2 K higher by 1200 h of day 2 (Fig. 7(a)),

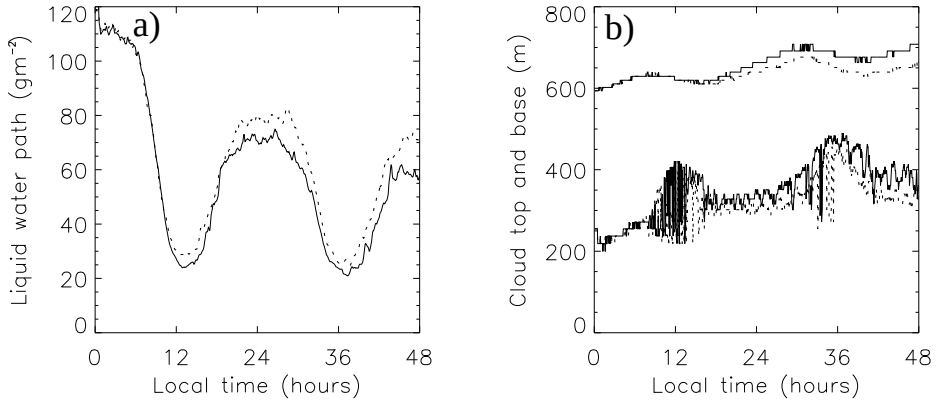

Figure 6. a) Liquid water path (g m^{-2}) and b) cloud top and cloud base (m), for the control simulation (solid line), and simulation 2-FT with absorbing aerosol above the inversion (dotted line).

consistent with the time-integrated aerosol shortwave heating rate. The increase in the strength of the capping inversion leads to a lower entrainment rate because the air above the inversion has a higher potential temperature and greater energy is required to "pull" this into the boundary layer. This leads to a shallower, moister BL with a higher LWP. For example, the BL was also 50 m shallower by the end of the simulation (Fig. 6(b)) and the total water was 0.2-0.3 g kg^{-1} higher in the upper half of the BL (Fig. 7(b)). The absorbing aerosol layer above the BL also reduces the down-welling solar flux reaching the cloud so that the shortwave heating rate at 1200 h is reduced by roughly 5%, or 1 K day^{-1} at cloud-top. It is possible that this cooling contributes to the increase in LWP.

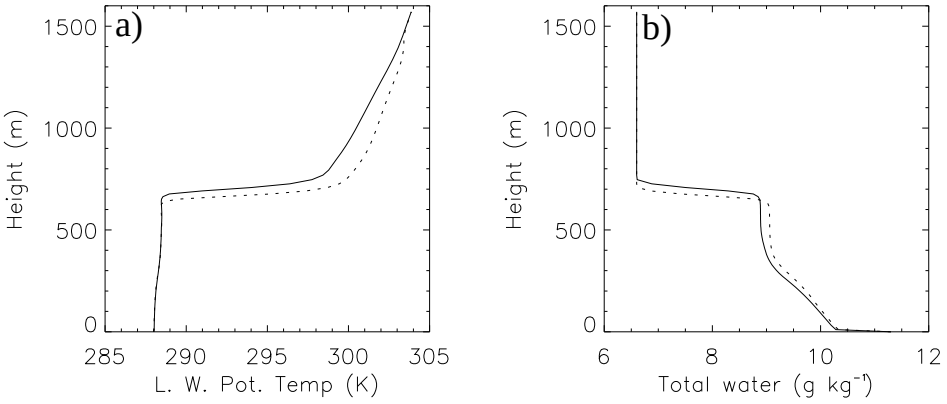

Figure 7. a) Liquid water potential temperature (K) and b) total water (g kg^{-1}) at 1200 h on day 2 in the control simulation (solid line), and experiment 2-FT with absorbing aerosol above the inversion (dotted line).

To test this hypothesis, a further experiment is performed with scattering aerosol above the inversion (experiment 2-FTS). This similarly reduced the down-welling shortwave radiation. We find a 0.5 K day^{-1} reduction in cloud-top shortwave heating

rate at 1200 h on account of the scattering aerosol. This is only half the reduction from absorbing aerosols with the same optical depth in experiment 2-FT, but if the increased LWP in experiment 2-FT is due to this reduced flux at cloud top, we might expect a small increase of LWP in experiment 2-FTS. However, the scattering aerosols had no significant impact on either the BL structure or the LWP leading to a negligible semi-direct aerosol effect (Table 3). This shows again, as in experiment 1-100 that the semi-direct aerosol effect depends only on shortwave absorption and heating. From the lack of response we can also infer that the semi-direct effect in experiment 2-FT was dominated, not by changes in absorbed solar radiation in the cloud, but by the suppression of entrainment due to the increase in temperature above the inversion.

With aerosols both in and above the BL (experiment 2-BLFT) the semi-direct aerosol forcing remains positive but is reduced to less than half that of the forcing when aerosols were only below the inversion (10 W m^{-2} compared to 23 W m^{-2}, Table 3). The difference (-13 W m^{-2}) is larger than the semi-direct aerosol effect with absorbing aerosols above the BL only (-10 W m^{-2}). This shows that there is some non-linearity. The aerosols above the BL cause a greater reduction in the semi-direct radiative forcing when there is aerosol below because they decrease the shortwave absorption not only of the cloud, but also of the absorbing aerosols in the BL.

The direct radiative forcing for absorbing aerosols above the BL is positive (10 W m^{-2}), and approximately cancels the negative semi-direct forcing (-9.5 W m^{-2}) so that the total radiative forcing is close to zero (Table 3). In contrast the direct radiative forcing from aerosol in the BL (exp. 2-BL) is small, and negative (-2.3 W m^{-2}). Aerosol above a reflective cloud layer absorbs far more solar radiative than aerosols below the cloud where the intensity of the radiation is lower (e.g. Haywood and Shine 1997). For example, the direct radiative forcing for aerosols above the inversion increases by 17.5 W m^{-2} (from -7.3 W m^{-2} to 10.2 W m^{-2}, Table 3), between the scattering and absorbing aerosol cases (experiments 2-FTS and 2-FT) for an optical depth of 0.2. This compares with an increase of only 2.3 W m^{-2} (Table 2) from the same reduction in ω for the aerosol layer in experiment 1, which is located mainly in the BL and has an optical depth of 0.15. Thus, the sign, magnitude, and relative importance of direct and semi-direct aerosol effects depend essentially on how much absorbing aerosol is within or above the cloudy BL. Hence, the semi-direct effect could be significantly affected by vertical advection or mixing of aerosols, or by the removal of aerosols from the BL by wet or dry deposition. Such processes will lead to more complex vertical distributions than those considered in this paper and the semi-direct aerosol effect is likely to vary quite widely depending on such factors.

5. CONCLUSIONS

Large-Eddy Simulations have been used to explore the semi-direct aerosol effect within the context of a marine stratocumulus-capped boundary layer. Stratocumulus covers about 20% of the globe and plays a major role in the climate system because of its high albedo relative to the ocean. The sensitivity of these clouds to absorbed solar radiation and the current lack of understanding of how aerosol absorption impacts this system motivates our study. We have chosen simplified aerosols types and vertical distributions to elucidate some of the basic mechanisms of the semi-direct effect. Particularly, we explore the dependence of the semi-direct effect on the aerosol single scattering albedo, and the vertical location of the aerosols relative to the cloud layer.

The key conclusions are as follows:

- It is found that moderately absorbing aerosol have a significant affect on stratocumulus LWP, leading to a strong semi-direct effect. This result was independent of the domain size or large-scale forcing used to drive the Large-Eddy Simulations. The semi-direct effect is proportional to the aerosol shortwave absorption, i.e. mid-visible single scattering co-albedo (1-ω) for the range: $0.88 < \omega < 1.00$, and for an aerosol optical depth of 0.15. However, the sign of the semi-direct effect depends on the vertical location of the aerosol layers relative to the inversion.

- For absorbing aerosols in the BL with τ = 0.12 and ω = 0.88, LWP is reduced by about 10 g m^{-2} leading to a large positive diurnal mean semi-direct forcing of up to 23 W m^{-2}, for the case of marine stratocumulus at 30^{o}N in July. The aerosols heat the cloud layer leading to evaporation and an enhancement of the daytime decoupling of the BL, reducing moisture fluxes between the surface and the cloud layer.

- Absorbing aerosol above the BL increases LWP leading to a negative semi-direct forcing of -10 W m^{-2} for τ = 0.20 and ω = 0.88. Heating of the air above the inversion leads to a lower entrainment rate and a shallower, moister BL.

- Scattering aerosol has no significant impact on the LWP whether located within or above the BL. It seems that the semi-direct effect depends only on the presence of absorbing aerosol material; in this case black carbon.

Previously it was assumed that the semi-direct effect was always positive (Hansen *et al.* 1997; Ackerman *et al.* 2000; Lohmann and Feichter 2001). We show the semi-direct effect could be negative if absorbing aerosol resides above the cloud layer. However, where absorbing aerosols are at the same level as the cloud, the semi-direct aerosol forcing is likely to be strong and positive. Clearly it is premature to suggest a likely range of values for the semi-direct effect, either locally or globally, because of the demonstrated sensitivity to the aerosol vertical distribution and to small scale BL processes. Also, because of the uncertainty in global distribution of aerosols and their optical properties it is more practical to compare estimates of the semi-direct forcing with the direct forcing. The previous studies (above) indicated that the semi-direct effect was less important than the direct effect other than for relatively high concentrations of absorbing aerosol.

This study shows that for marine stratocumulus, even for moderately absorbing aerosols, the semi-direct forcing may far exceed the direct forcing. For aerosols in the BL, the variation of semi-direct forcing with ω is 6 times greater than the variation of direct radiative forcing. This shows that absorbing aerosol material such as black carbon potentially has a much greater impact on radiative forcing than estimated from its direct

forcing alone. Also, the total aerosol radiative forcing (excluding indirect effects) was found to be positive for aerosols with $\omega < \omega_{**} = 0.985$. This is in the upper range of typically observed mid-visible ω values (IPCC, 2001) suggesting that, excluding indirect effects, even weakly absorbing aerosols could have a positive radiative forcing. Hansen *et al.* (1997) find a much lower value of ω_{**} in their general-circulation model study (0.91 compared to 0.985 in our study). This suggests either that the semi-direct effect is model dependent or that marine stratocumulus is particularly sensitive to absorbing aerosols.

This study illustrates that the semi-direct aerosol effect is intimately linked to small scale processes such as turbulent fluxes, entrainment and the decoupling of the BL. The semi-direct effect is therefore likely to depend to a large extent on local meteorological conditions. For example Ackerman *et al.* (2000) found a much smaller semi-direct forcing (3 W m^{-2} compared to 16 W m^{-2}) for the trade cumulus boundary layer using LES and a similar aerosol concentration and mid-visible single scattering albedo. Similar studies using a range of different meteorological conditions, and observed aerosols are needed to understand further the way the semi-direct aerosol effect works locally. Ultimately though, estimation of the global mean forcing requires large-scale models. It is therefore important to establish whether global models are capable of treating the interaction between the aerosol heating rate and the small-scale dynamic processes affecting cloud properties, for example, convection, turbulence and cloud-top entrainment.

Stratocumulus is poorly resolved in large-scale models and the diurnal cycle of LWP is underestimated because the BL decoupling process is not sufficiently represented in the models (e.g. Grenier and Bretherton 2001). This would lead to an underestimation of the semi-direct effect from absorbing aerosols in cloudy boundary layers. Therefore, verification of global models with high resolution cloud resolving or large-eddy resolving models will be important in developing our understanding of the semi-direct aerosol effect.

In this study there was no possibility for interaction between the aerosols and cloud microphysics or radiative properties, nor have we allowed the sea surface temperature to respond to the aerosols or changes in cloud fields. To assess the full role of absorbing aerosols on climate, additional mechanisms need to be included, such as the interaction between aerosols and microphysics, and impacts on sea surface temperature and the large-scale flow (Chung *et al.* 2002). Future studies of the semi-direct effect need to consider the impact of such factors.

ACKNOWLEDGEMENTS

We would like to thank the Natural Environment Research Council (NERC) for funding both BTJ and PMF, the Met Office for providing the Large-Eddy-Model (LEM), Marc Stringer at the University of Reading for his assistance in using the LEM, and the referees for their useful comments.

REFERENCES

Ackerman, A. S., Toon, O. B., Stevens, D. E., Heymsfield, A. J., Ramanathan, V. and Welton, E. J. 2000 Reduction of tropical cloudiness.*Science,***288,** 1042-1047

Betts, A. K. 1990 Diurnal variation of Californian coastal stratocumulus from two days of boundary layer soundings.*Tellus,***42A,** 302-304

Brown, A. R. 1999 The sensitivity of large-eddy simulations of shallow cumulus convection to resolution and subgrid model. *Q. J. R. Meterol. Soc.*, **125,** 469–482

Chung, C. E., Ramanathan, V., and Kiehl, J. 2002 Effects of the south Asian absorbing aerosol haze on the northeast monsoon and surface-air heat exchange. *J. Clim*, **15**, 2462–2476

Chylek, P., Lesins, G. B., Videen, G., Wong, J. G. D., Pinnick, R. G., Ngo, D., and Klett, J. D. 1996 Black carbon and absorption of solar radiation by clouds. *J. Geophys. Res*, **101**, 23365–23371

Clarke, A. D., Porter, J. N. and Valero, F. P. J. 1996 Vertical profiles, aerosol microphysics, and optical closure during the Atlantic Stratocumulus Transition Experiment: Measured and modeled column optical properties. *J. Geophys. Res.*, **101,** 4443-4453

Cook, J. and Highwood, E. J. 2003 Climate response to tropospheric absorbing aerosol in an Intermediate General-Circulation Model. *Q. J. R. Meteorol. Soc. in press.*

Duynkerke, P. G. and Hignett, P. 1993 Simulation of diurnal variation in a stratocumulus-capped marine boundary layer. *Mon. Weather Rev.*, **121,** 3291–3300

Duynkerke, P. G., Jonker, P. J. and Van Dijk, A. 2000 FIRE I observations for the model intercomparison of EUROCS: Stratocumulus over the ocean. Institute for Marine and Atmospheric Research Utrecht (IMAU) Utrecht University, Princetonplein 5, 3584 CC Utrecht, The Netherlands.

Duynkerke, P. G. and Teixeira, J. 2001 Comparison of the ECMWF Reanalysis with FIRE I Observations. *J. Clim.*, **14,** 1466–1478

Edwards, J. M. and Slingo, A. 1996 Studies with a flexible new radiation code: 1. Choosing a configuration for a large-scale model. *Q. J. R. Meteorol. Soc.*, **122,** 689–719

Gray, M. E., Petch, J., Derbyshire, S. H., Brown, A. R., Lock, A. P., Swann, H. A. and Brown, P. R. A 2001 Version 2.3 of the Met Office Large-Eddy Model: Part II. Scientific documentation. MET O (APR) Turbulence and Diffusion report 276. Met Office, Bracknell, UK.

Grenier, H. and Bretherton, C. S. 2001 A moist PBL parameterisation for large-scale models and its application to subtropical cloud-topped marine boundary layers. *Mon. Weather Rev.*, **129,** 357–378

Hansen, J. E., Sato, M. and Ruedy, R. 1997 Radiative forcing and climate response *J. Geophys. Res.*, **102,** 6831–6864

Haywood, J. M. and Boucher, O. 2000 Estimates of the direct and indirect radiative forcing due to tropospheric aerosols: A review. *Rev. Geophys.*, **38,** 513–543

Haywood, J. M. and Shine, K. P. 1997 Multi-spectral calculations of the direct radiative forcing of tropospheric sulphate and soot aerosols using a column model. *Q. J. R. Meteorol. Soc.*, **123,** 1907–1930

Haywood, J. M., Osborne, S. R., Francis, P., Keil, A., Formenti, P., Andreae, M. and Kaye, P. 2003 The mean physical and optical properties of regional haze dominated by biomass burning aerosol measured from the C-130 aircraft during SAFARI-2000. *J. Geophys. Res.*, **108,** 8473, doi:10.1029/2002JD002226

Heintzenberg, J., Charlson, R. J., Clarke, A. D., Liousse, C., Ramanathan, V., Shine, K. P., Weindisch, M. and Helas, G. 1997 Measurements and modelling of aerosol single-scattering albedo: Progress, problems and prospects.*Beitr. Phy. Atmosph.*, **70**(4), 249–263

Hignett, P. 1991 Observations of diurnal variation in a cloud-capped marine boundary layer. *J. Atmos. Sci.*, **48,** 1474–1482

Huebert, B. J., Pszenny, A. and Blomquist, B. 1996 The ASTEX/MAGE experiment. *J. Geophys. Res.*, **101,** 4319–4329

IPCC 2001 Climate change 2001: Scientific basis. Third assessment report of the Inter-governmental Panel on Climate Change (IPCC). *Cambridge.*

Jacobson, M. Z. 2002 Control of fossil-fuel black carbon and organic matter, possibly the most effective method for slowing global warming *J. Geophys. Res.*, **107,** 4410, doi:10.1029/2201JD001376

Johnson, D. W., Osborne, S. R., Wood, R. Suhre, K., Johnson, R., Businger, S., Quinn, P. K., Wiedensohler, A., Durkee, P. A., Russell, L. M., Andreae, M. O., Noone, K. J., Bandy, B., Rudolph, J., O'Dowd, C. and Rapsomanikis, S. 2000a An overview of the lagrangian experiments undertaken during the North Atlantic regional aerosol characterisation experiment (ACE-2). *Tellus,* **52b,** 290–320

Johnson, D. W., Osborne, S. R., Wood, R. Suhre, K., Quinn, P. K., Bates, T., Andreae, M. O., Noone, K. J., Glantz, P., Bandy, B., Rudolph, J. and O'Dowd, C. 2000b Observations of the evolution of the aerosol, cloud and boundary layer characteristics during the 1st ACE-2 Langrangian experiment. *Tellus*, **52b,** 348–374

Krueger, S. K., McLean, G. T. and Fu, Q. 1995 Numerical simulations of the stratus-to-cumulus transition in subtropical marine boundary layers. Part I: Boundary layer structure. *J. Atmos. Sci.*,**52,** 2839–2850

Lock, A. P. and Macvean. M. K. 1999 The parameterisation of entrainment driven by surface heating and cloud-top cooling. *Q. J. R. Meteorol. Soc.,* **124,** 271–299

Lohmann, U. and Feichter, J. 2001 Can the direct and semi-direct compete with the indirect aerosol effect on a global scale? *Geophys. Res. Lett.,* **28,** 159–161

Mason, P. J. 1989 Large-eddy simulations of the convective atmospheric boundary layer. *J. Atmos. Sci.* **46,** 1492–1516

Moeng, C. H. 2000 Entrainment rate, cloud fraction, and liquid water path of PBL stratocumulus. *J. Atmos. Sci.* **57.** 3627–3643

Nicholls, S. 1984 The dynamics of stratocumulus: Aircraft observation and comparison with a mixed layer model. *Q. J. R. Meteorol. Soc.*, **110,** 783–820

Penner, J. E. and Zhang, S. Y. 2003 Soot and smoke may not warm climate. *J. Geophys. Res.*,**108**(D21), 4657, doi: 10/1029/2003/JD003409

Pilinis, C., Pandis, S. N. and Seinfeld, J. H. 1995 Sensitivity of direct climate forcing by atmospheric aerosol to aerosol-size composition. *J. Geophys. Res.,* **100,** 18739–18754

Ramanathan, V., Crutzen, P. J. and Rossenfeld, D. 2001 Aerosols, climate and the hydrological cycle. *Science,* **294,** 2119–2124

Russell, P. B., Redemann, J., Schmid, B., Bregstrom, R. W., Livingstone, J. M., McIntosh, D. M., Ramirez, S. A., Hartley, S., P.V.Hobbs, Quinn, P. K., Carrico, C. M., Rood, M. J., Ostrom, E., Noone, K. J., vov Hoyningen-Huene, W., and Remer, L. 2002 Comparison of aerosol single scattering albedos derived from diverse techniques in two North Atlantic experiments. *J. Atmos. Sci.,* **59**, 609–619

Satheesh, S. K. and Ramanathan, V. 2000 Large differences in tropical aerosol forcing at the top of the atmosphere and Earth's surface. *Nature,* **405**, 60–62

WCP 1986 A preliminary cloudless atmosphere for radiation computation. Technical Report WCP-112, WMO/TD-BO.24, World Meteorological Organisation, Geneva.